STM JOURNALS

International Journal of
Fracture Mechanics and
Damage Science

Volume 4, Issue 1, 2026
January–June
DOI (Journal): 10.37591/IJFMDS

https://journals.stmjournals.com/ijfmds

Review IJFMDS

Impact of Fracture in Geometrical, Material, and Load Rate Characteristics on J-Integral

Piyush Goyal[1,*], Hridyanshu[1]

Abstract

The present study investigates the influence of load rate, geometrical parameters, and material properties on the J-integral behavior of AA2050-T84 aluminum-lithium alloy using three-dimensional elastic–plastic fracture mechanics (EPFM) analysis. Finite element simulations were carried out using the ABAQUS software to evaluate crack driving forces in compact tension (C(T)) specimens under various mechanical and thermal conditions. The study focuses on the combined effects of strain rate, temperature-dependent strain hardening, specimen thickness (B/W ratio), and material anisotropy on J-integral variation along the crack front. A multilinear kinematic hardening material model derived from true stress–strain data was employed to accurately represent plastic deformation behavior. The numerical results were validated through comparison with experimental load versus crack mouth opening displacement (CMOD) curves, confirming the reliability of the developed model. The analysis revealed that the J-integral reaches its maximum value at the crack front center due to crack tunneling effects. Although strain rate showed a positive dependency on J-integral, its influence remained minimal within quasi-static ranges. The results also indicated that J-integral increases with increasing strain hardening ratio and decreases with increasing specimen thickness due to higher constraint effects. Furthermore, anisotropy significantly affected fracture behavior depending on plate orientation and location. These findings provide valuable insights into fracture characterization and structural reliability of Al-Li alloy components used in aerospace structures.

Keywords: J-integral, elastic–plastic fracture mechanics (EPFM), AA2050-T84 alloy, finite element analysis, ABAQUS simulation

INTRODUCTION

The restriction of SSY was not ideal for finding the fracture toughness of ductile materials. In EPFM, the large plasticity ahead of crack considered for crack characterization. J-integral and the CTOD have been utilized for defining the fracture toughness in EPFM. Various researchers [1–3] have reported the significance of the J-integral assessment in crack tip plasticity driven ductile materials. The J-integral measurement techniques have been almost identical in various standard bodies [4, 5] across the world. ASTM E1820-20a [5], also recognized the JIC and J-R curve for the quantifying the crack behavior, for defined specimen dimension restrictions. However, in practical applications, the variations in material, and geometrical property along with environmental temperature alter the crack behavior of the component. The alteration of crack front field can be accounted through J or δ and a constraint parameter. Unlike J- integral estimation, CTOD involved complexity and diversity in its estimation across the different standards. Hence, the CTOD usage as a fracture parameter was restricted in

***Author for Correspondence**
Piyush Goyal
E-mail: Piyushgoyal@eitfaridabad.co.in

[1]Research Scholar, Department of Mechanical Engineering, Echelon Institute of Technology, Faridabad, Haryana, India

Received Date: March 25, 2026
Accepted Date: March 26, 2026
Published Date: April 07, 2026

Citation: Piyush Goyal, Hridyanshu. Impact of Fracture in Geometrical, Material, and Load Rate Characteristics on J-Integral. International Journal of Fracture Mechanics and Damage Science. 2026; 4(1): 38–45p.

practical applications. Therefore, the CTOD estimation methods and its relation with J- integral is dealt in next chapter. In this chapter, the investigation is to address the following major objectives.

(a) To compute the J-integral in AA2050-T84 alloy made C(T) specimen using 3D EPFM analyses.
(b) To study the effect of SR, and test temperature (or yield to tensile strength ratio) on J-integral.
(c) To evaluate the specimen thickness effect (B) on J-integral variation along the crack front.
(d) To examine AA2050-T84 alloy plate anisotropy effect on J-integral variation under the applied load.

FE Details

The SR and temperature variations were considered while performing the three-dimensional FE immolations using C(T) specimen. The following sections elucidate the considerations of material property, geometry, and boundary conditions used in modeling and analysis.

Material and Specimen Geometry

In case of EPFM analyses, material deformation was considered as multi-linear kinematic hardening type. The uncertain nature of the alloy beyond the yield point conceivably well- understood and modelled using kinematic hardening type. The details of the kinematic hardening type material were given in Appendix E. By dividing the $\sigma true$ - $\varepsilon true$ curve of the material into 20 divisions, the material's reaction to plastic deformation has been predicted. In the model, it was expected that the plastic deformation between two adjacent locations would be linear and have a specific tangent modulus. A typical multilinear model (extracted from AA2050-T84 alloy true stress-strain curve obtained at 0.01 s^{-1} strain rate and test temperature of 200^0 C) used in the present FEA is illustrated in Figure 1. The load stages were represented in the form of normalized applied stress or stress ratio (□/□y). The ABAQUS post-processor was used to obtain *J*-integral values for each load phase. The method of extraction of *J* has been explained in the Section 1.2.3.

FE Mesh and Boundary Conditions

Elastic-plastic FEA includes nonlinear plasticity conditions to elastic analysis [6]. The FE mesh and BC's for 3D C(T) specimens were generated in a similar manner as carried-out in LEFM analysis. The FE meshes induced around the crack. The 3D analyses domains were divided using 20-noded quadratic brick finite elements with reduced integration (element type C3D20R within ABAQUS library). Figure 2 shows a typical meshed C(T) specimen with boundary conditions. Eleven layers along the crack front were used in this FEA to calculate the J. The B dimension, considered in these analyses varied as 2.54 mm, 12.7 mm and 25.4 mm. Similarly, the examined temperatures were varied as -200 C, 240 C, and 2000 C along with quasi-static load rates.

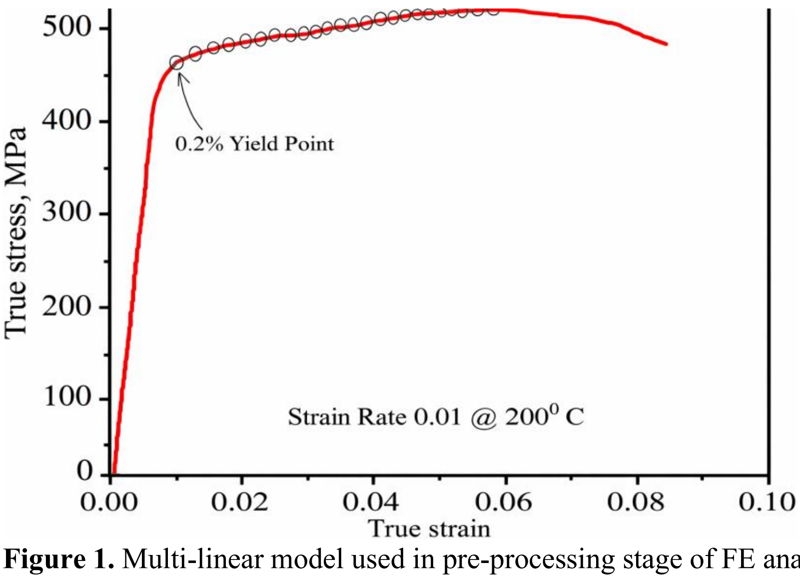

Figure 1. Multi-linear model used in pre-processing stage of FE analysis.

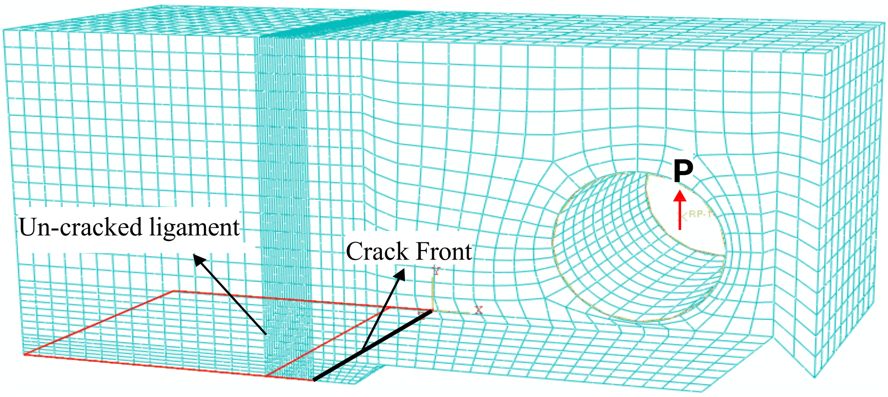

Figure 2. A symmetric C(T) specimen meshed model with boundary conditions.

Computation of J

The J computation using FE analysis were identical to the early literature reports [7]. Employing the domain integral method, the J was computed for a defined path around the crack, usually set manually in the ABAQUS software. The path-independency of the J helped to obtain the J values beyond the process zone of the crack field. The methods to estimate the J [8–10] were integrated to ABAQUS software. These simple and effective methods to evaluate the J do not depend on the mesh size level and type [8]. The detailed extraction methods of J for 2D and 3D are given Appendix F.

By default, ABAQUS uses the iterative solver to solve nonlinear equations during J-integral computation. The modified Newton-Raphson method is used in ABAQUS, which iteratively improves the convergence criteria are met. For most nonlinear J-integral calculations this method sufficiently provides good accuracy. The load step size in EPFM fracture analysis is chosen such that the analysis is stable and converges to a solution that accurately predicts the behavior of the material under the given loading conditions.

The load step size is often adjusted during the analysis to ensure that the solution is accurate and stable. In our case both fixed and automatic increments are used depending upon the requirements. Reduced integration is a technique used in finite element to reduce the number of integration points used in the numerical integration of element stiffness matrices. It also reduces the occurrence of spurious mesh sensitivity and locking. This can result in reduced computational costs and improved numerical stability, especially in the presence of stress singularities.

METHODOLOGY

In the present 3D analysis, the ABAQUS instinctively locates user defined contours to determine J-integral. Few contours nearer to the crack couldn't estimate the persistent J values due to process zone [7]. Hence, in the current analysis, first two contours were neglected to obtain persistent magnitudes of J. The average of last three contours of J values were estimated for nodes along the crack front. The J-integral was extracted for various SR, temperatures and B for a/W = 0.5.

The numerical model of EPFM analysis was verified by evaluating the load vs. CMOD plots with experimental results. The validation of the numerical model can be verified by CMOD is the linear displacement between knife edge points on the standard fracture specimen and can be measured by clip gauges.

A typical CMOD measurement in 3D numerical analysis is shown in Figure 3. The comparison between load versus CMOD or COD of experimental and numerical values for different temperatures is shown in Figure 4. A sharp crack tip/front was used for numerical analyses as opposed to blunted crack tip/front usage in a few of the literature studies for SEN(B) specimens [8, 9].

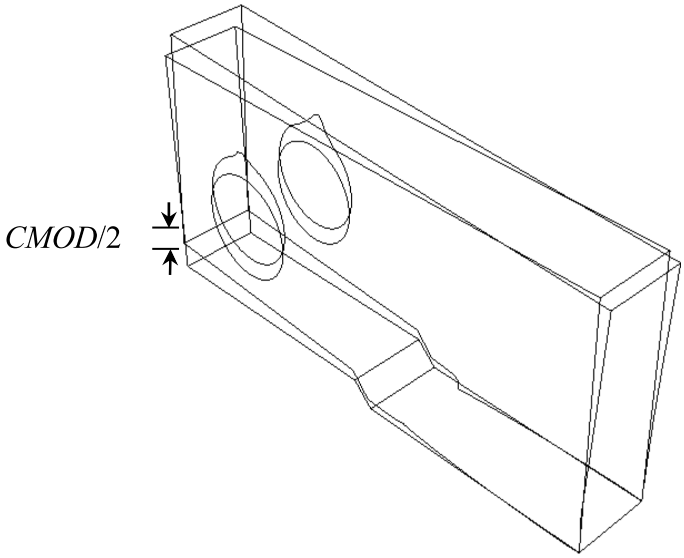

Figure 3. Measurement of *CMOD* from symmetrical C(T) specimen.

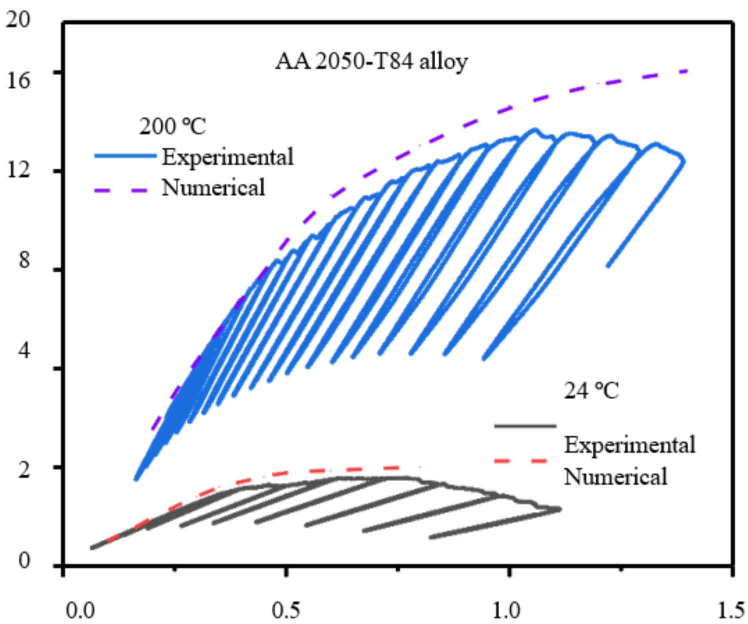

Figure 4. Comparison between experimental and numerical Load versus *CMOD.*

Like the blunted crack, a sharp crack cannot account for the crack propagation as seen during experimental tests. However, the effective usage of a sharp crack in earlier literature [10] for the C(T) specimen can be found for accurate CTOD measurement. Moreover, Figure 5 depicts the similarity between numerical results with experimental load versus CMOD values (for the most part) to justify the current procedure of analyzing the C(T) model. From Figure 5, the deviation of experimental and numerical curves after the CMOD value of around 0.4 can be noticed. The deviation in numerical curve from experimental may be attributed to blunting of the crack usually observed in experimental tests [8, 9]. Overall, the load vs. CMOD data variations for different temperatures for the identical alloy is the indication of reliability on geometry dependent behavior of the alloy. At 24 0C, the specimen width was considered in experimental fracture study was 25.4 mm and that for 200 0C, it was 50.8 mm. Similar to variation in stress-strain behavior for both temperatures, here the resistance to applied load depends on crack size and specimen geometry.

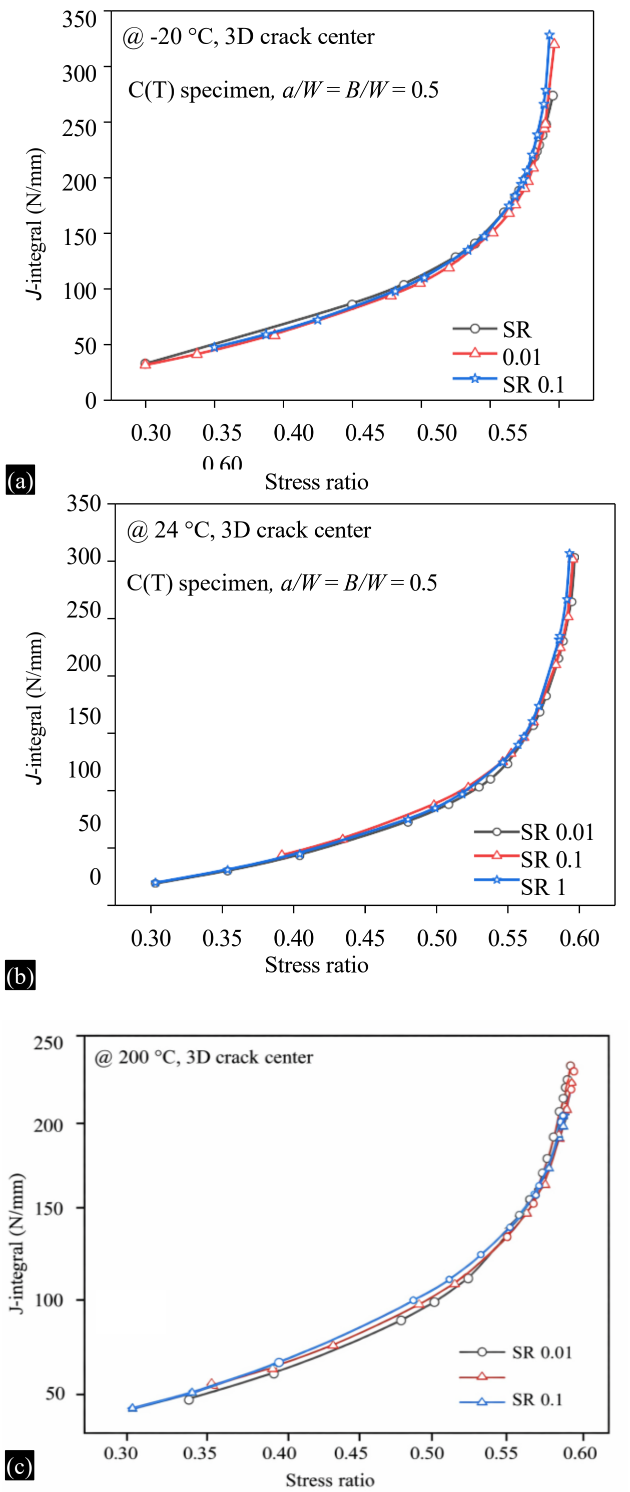

Figure 5. *J*-integral versus stress ratio at quasi-static strain rates for (a) -20^0 C (b) 24^0 C (c) 200^0 C.

Hence, these variations are seen in Figure 5. However, the numerical applied loads are quite similar to experimental load patterns, thus indicative of validation of current EPFM procedure. Also, the J-integral values were compared to the earlier work [11–13] to validate the current analysis procedure.

Further, the J values were extracted along the crack front and found to be maximum at the crack center. Thus, for comparison further, crack front center values of J-integral were used.

Effect of Strain Rate on J-Integral

It has been observed in tensile testing that quasi-static strain rate variation resulted serrated stress-strain curves. While, the LEFM parameters (K_I and T-stresses) have shown the negligible variation due to change in lower SR. The negligible variation in elastic fracture behavior was attributed to identical ν and E values at different strain rates. However, in σ_{true} - ε_{true} curve the post yield behavior of varied SR were noticeable. As a result, the influence of SR change on J variation was examined in the current section.

The standard C(T) specimen was built and analyzed at identified temperatures under lower SR. The variation of J-integral (at crack center) for the applied stress ratio at lower SR was correlated, as seen in Figure 5. The variation of J-integral was minimal between the SR for examined temperatures.

Further, the nature of J-integral variation was non-linear for all strain rates. Meanwhile, a direct association among J-integral and stress ratio can be witnessed up to a stress ratio of around 0.45. Similar nature of J-integral variations was also observed for other specimen thicknesses (B/W = 0.1 and 1). In the ordered sequence of $0.01 < 0.1 < 1$ s^{-1}, the maximum J-integral values were seen at SR 1 s^{-1}. Therefore, one can conclude that the positive SR dependency of crack driving parameters in both LEFM and EPFM analysis of AA2050-T84 alloy.

Similarly, the recommendation of using identical J_{IC} for quasi-static strain rates variations by ASTM 1820-20a seems correct. Since the SR dependency was minimal on J-integral, further, the effect of anisotropy, temperature and specimen thickness were restricted to strain rate 0.1 s^{-1} only.

Influence of Temperature (Strain Hardening) on J-Integral

The temperature effect at SR 0.1 s^{-1} can be better represented as strain hardening values. The strain hardening of the alloy at different test temperature was denoted in terms of yield to ultimate strength ratio (σ_{ys} / σ_{ut}). The variation of σ_{ys} / σ_{ut} of the present considered alloy. The σ_{ys} / σ_{ut} values at strain rate 0.1 s^{-1}, at considered temperatures were calculated. The test temperatures -200 C, 240 C, and 2000 C were computed as 0.87, 0.84 and 0.90 in terms of σ_{ys} / σ_{ut}. In literature [8, 9, 5, 14], the influence of strain hardening on EPFM parameters, J-integral and CTOD were reported.

However, in most of these studies, the strain hardening values were assumed and not derived from any real materials. Hence, the need of strain hardening effect on J-integral for different specimen B/W (representing practical components thicknesses) as thin, standard and thick was essential to understand the real crack behavior. The variation of J-integral versus stress ratio in different strain hardening materials and specimen thicknesses are shown in Figure 6. It was noticed from Figure 6 that the natures of variations of J-integral for all the considered σ_{ys} / σ_{ut} were identical and non-linear. The J-integral of the alloy increased with increase in σ_{ys} / σ_{ut}.

However, the difference in J-integral magnitude between 0.87 and 0.90 of σ_{ys} / σ_{ut} was minimal (almost negligible) in all the thicknesses considered. Meanwhile, the difference in the σ_{ys} / σ_{ut} of 0.84 and 0.87 (or 0.90) seems to be higher in thin specimen compared to standard and thick cases. The stress ratio of 0.45 as a reference value was considered (refer Figure 6) for comparison between the different specimens. At a constant stress ratio (= 0.45), between the 0.84 and 0.87 (or 0.90) of σ_{ys} / σ_{ut}, an increase of around 26%, 20% and 18% in thin, standard and thick specimens were noticed respectively.

Thus, the J-integral sensitivity was dependent on both test temperature (strain hardening of the alloy) and specimen thickness. It can be inferred that at a constant stress ratio, the variation in J-integral depends on strain hardening of the alloy. Notably, the specimen thickness associated crack front stress fields can be the primary reason and will be discussed in detail in further chapter with the help of constraint parameter.

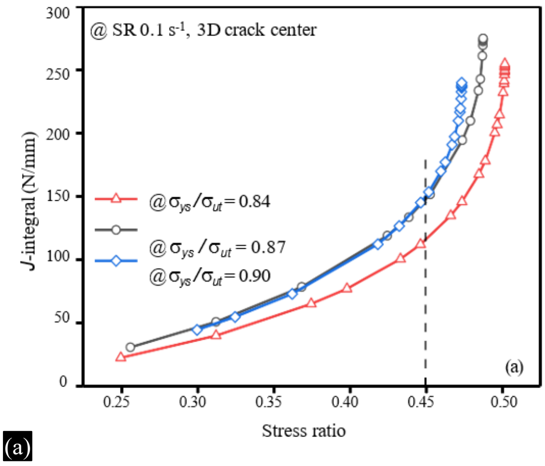

(a)

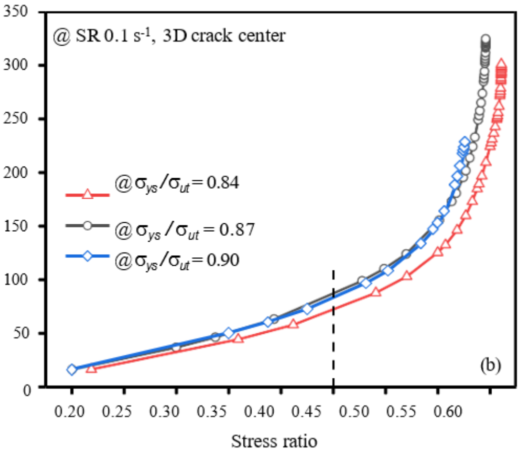

(b)

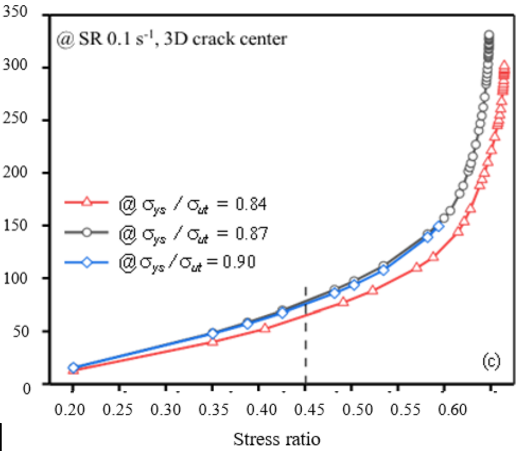

(c)

Figure 6. J-integral versus Stress ratio at various yield to ultimate strength ratios for B/W of (a) 0.1 (b) 0.5 (c) 1

CONCLUSIONS

In this investigation, the influence of strain rate, temperature, specimen thickness and anisotropy of the alloy on *J*-integral variation was studied. The effect of temperature was discussed in terms of strain hardening of the alloy, represented as yield to ultimate strength ratio ($\sigma ys\ /\ \sigma ut$). The thin, standard and thick C(T) specimens were used to verify the *J*-integral variations. Also, the main focus was given to combined effect of above parameters (strain rate, temperature, specimen thickness and anisotropy) on *J*-integral. Following are the conclusions drawn from the present investigation:

- The magnitude of *J*-integral varies along the crack-front for C(T) specimen and maximum value noticed at the crack front center for all the specimen thicknesses.
- Positive strain rate dependency of *J*-integral was witnessed for all quasi static strain rates. However, *J*-integral variation between the quasi-static strain rates is minimal for all specimen thickness and temperatures.
- The *J*-integral of the alloy increases with increase in $\sigma_{ys} / \sigma_{ut}$ and relatively more sensitive in thin specimens.
- The *J*-integral magnitude was decreased beyond the standard specimen thickness.
- Anisotropy effect on *J*-integral was measured at different plate locations and orientations. Plate surface (t/6) location exhibited isotropic behavior irrespective of plate orientations for both room and cryogenic temperatures.

REFERENCES

1. J. R. Rice, “A path independent integral and the approximate analysis of strain concentration by notches and cracks,” Journal of Applied Mechanics, vol. 35, no. 2, pp. 379–386, 1968.
2. J. R. Rice and G. F. Rosengren, “Plane strain deformation near a crack tip in a power-law hardening material,” Journal of the Mechanics and Physics of Solids, vol. 16, no. 1, pp. 1–12, 1968.
3. C. F. Shih, “Relationships between the J-integral and the crack opening displacement for stationary and extending cracks,” Journal of the Mechanics and Physics of Solids, vol. 29, no. 4, pp. 305–326, 1981.
4. ISO 12135, Metallic Materials — Unified Method of Test for the Determination of Quasi-Static Fracture Toughness, International Organization for Standardization, Geneva, Switzerland, 2016.
5. ASTM E1820-20a, Standard Test Method for Measurement of Fracture Toughness, ASTM International, West Conshohocken, PA, USA, 2020.
6. O. C. Zienkiewicz and R. L. Taylor, The Finite Element Method: Its Basis and Fundamentals, 7th ed. Oxford, U.K.: Butterworth-Heinemann, 2013.
7. ABAQUS Documentation, ABAQUS Analysis User’s Manual, Version 6.14, Dassault Systèmes Simulia Corp., Providence, RI, USA, 2014.
8. J. W. Hutchinson, “Singular behaviour at the end of a tensile crack in a hardening material,” Journal of the Mechanics and Physics of Solids, vol. 16, no. 1, pp. 13–31, 1968.
9. M. F. Kanninen and C. H. Popelar, Advanced Fracture Mechanics. New York, NY, USA: Oxford University Press, 1985.
10. J. D. Landes and J. A. Begley, “A fracture mechanics approach to creep crack growth,” Mechanics of Crack Growth, ASTM STP 590, pp. 128–148, 1976.
11. A. Saxena, Nonlinear Fracture Mechanics for Engineers. Boca Raton, FL, USA: CRC Press, 1998.
12. T. L. Anderson, Fracture Mechanics: Fundamentals and Applications, 4th ed. Boca Raton, FL, USA: CRC Press, 2017.
13. J. C. Newman and I. S. Raju, “Stress-intensity factor equations for cracks in three-dimensional finite bodies,” Engineering Fracture Mechanics, vol. 15, no. 1–2, pp. 185–192, 1981.
14. M. L. Williams, “On the stress distribution at the base of a stationary crack,” Journal of Applied Mechanics, vol. 24, no. 1, pp. 109–114, 1957.

